land

MDPI

Article

Analyzing the Accuracy of Satellite-Derived DEMs Using High-Resolution Terrestrial LiDAR

Aya Hamed Mohamed *, Mohamed Islam Keskes and Mihai Daniel Nita *

Faculty of Silviculture and Forest Engineering, Transilvania University of Braşov, Şirul Ludwig van Beethoven 1, 500123 Braşov, Romania; mohamed.keskes@unitbv.ro

* Correspondence: aya.hamed@unitbv.ro (A.H.M.); mihai.nita@unitbv.ro (M.D.N.)

Abstract: The accurate estimation of Digital Elevation Models (DEMs) derived from satellite data is critical for numerous environmental applications. This study evaluates the accuracy and reliability of two satellite-derived elevation models, the ALOS World 3D and SRTM DEMs, specifically for their application in hydrological modeling. A comparative analysis with Terrestrial Laser Scanning (TLS) measurements assessed the agreement between these datasets. Multiple linear regression models were utilized to evaluate the relationships between the datasets and provide detailed insights into their accuracy and biases. The results indicate significant correlations between satellite DEMs and TLS measurements, with adjusted R-square values of 0.8478 for ALOS and 0.955 for the SRTM. To quantify the average difference, root mean square error (RMSE) values were calculated as 10.43 m for ALOS and 5.65 m for the SRTM. Additionally, slope and aspect analyses were performed to highlight terrain characteristics across the DEMs. Slope analysis showed a statistically significant negative correlation between SRTM and TLS slopes ($R^2 = 0.16$, $p < 4.47 \times 10^{-10}$ indicating a weak relationship, while no significant correlation was observed between ALOS and TLS slopes. Aspect analysis showed significant positive correlations for both ALOS and the SRTM with TLS aspect, capturing 30.21% of the variance. These findings demonstrate the accuracy of satellite-derived elevation models in representing terrain features relative to high-resolution terrestrial data.

Keywords: satellite-derived elevation models; terrestrial laser scanning (TLS); spatial data validation; topographic data

Citation: Mohamed, A.H.; Keskes, M.I.; Nita, M.D. Analyzing the Accuracy of Satellite-Derived DEMs Using High-Resolution Terrestrial LiDAR. *Land* **2024**, *13*, 2171. https://doi.org/10.3390/land13122171

Academic Editor: Todd Robinson

Received: 7 November 2024
Revised: 9 December 2024
Accepted: 10 December 2024
Published: 13 December 2024

1. Introduction

Digital Elevation Models (DEMs) represent a fundamental component of geospatial data, providing critical insights into the Earth's surface topography [1–3]. These models offer a comprehensive view of our planet's terrain, from towering mountains to sprawling valleys and intricate water bodies [4]. The applications of DEMs are far-reaching, spanning from land use planning and natural resource management to environmental modeling [5,6]. To acquire DEM data, satellite-derived products have become a widely utilized resource due to their large area coverage and spatial resolution capabilities. However, it is crucial to recognize that the accuracy of these satellite-derived products can fluctuate considerably due to several factors [1,7]. These factors encompass sensor characteristics, atmospheric conditions, and processing algorithms, all of which can influence the quality of the data utilized in hydrological modeling [5].

One notable limitation of satellite sensors is their spatial resolution, coupled with their susceptibility to atmospheric interference [8]. Satellite-based remote sensing relies on capturing reflected or emitted electromagnetic radiation from the Earth's surface.

Nonetheless, this process can be impacted by factors such as cloud cover, atmospheric conditions, and the sensor's spatial resolution [8,9]. Consequently, the DEM data derived from satellites may exhibit lower accuracy and resolution when compared to ground-based measurements. Despite these inherent limitations, satellite sensors offer a range of

invaluable advantages [10,11]. They provide extensive coverage and repetitive observations, rendering them ideal for large-scale assessments and long-term monitoring efforts. These characteristics make satellite-derived products particularly valuable for the study and monitoring of environmental changes over vast geographical areas [10,12].

The Shuttle Radar Topography Mission (SRTM) and the Advanced Land Observation Satellite (ALOS) stand as exemplary satellites that have significantly contributed to the collection of topographic data [13,14]. The Shuttle Radar Topography Mission (SRTM) was a groundbreaking NASA-led international effort made in February 2000 to acquire the elevation data of the Earth's surface using synthetic aperture radar (SAR) technology. A specially modified radar system was deployed aboard the Space Shuttle Endeavour for this mission [15]. The SRTM utilized radar instruments, namely the Spaceborne Imaging Radar-C (SIR-C) and the X-band Synthetic Aperture Radar (X-SAR), to transmit radar signals to Earth's surface. SRTM elevation models are widely used in geographic information systems (GISs) and are easily accessible for download, bolstered by support from various software platforms, making them a preferred choice for elevation analysis and mapping in both academic and professional contexts [13,16].

Another satellite that has played a pivotal role in the collection of topographical data is the Advanced Land Observation Satellite (ALOS) [17]. Launched on 24 January 2006, by the Japan Aerospace Exploration Agency (JAXA) [18], ALOS was equipped with an array of sensors and instruments designed to gather comprehensive data on the Earth's surface [19]. These instruments included the Digital Surface Model (DSM), Multi-look Scan-SAR (MSK), Land Surface Temperature (LST), High Dynamic Range (HDR), Original Image (ORI), and Calibrated Radiometric Image (CCI), enabling scientists to capture a wealth of information about the Earth's surface, including elevation data, temperature measurements, and high-quality images [20,21]. ALOS operated successfully for five years until it encountered an anomaly in power generation, leading to its termination on 12 May 2011, as reported by Short [22]. Nevertheless, approximately 6.5 million scenes of archived data from ALOS remain available, covering the entire globe and serving as a valuable resource for various geospatial applications. ALOS furnished critical information on elevation, captured wide-area images, measured land surface temperatures, and provided images with a broader range of brightness levels [23].

In accordance with Zhang [24], an effective method for enhancing the precision of satellite-derived products involves the integration of terrestrial LiDAR measurements. TLS technology operates based on the principle of time-of-flight measurement, as explained by Suchocki [25]. The scanner emits a laser beam and measures the time taken for the beam to travel to the scanned object and return to the scanner. Utilizing the speed of light and time-of-flight measurement, the distance between the scanner and the object can be calculated. To scan the object, TLS devices typically incorporate a rotating mirror that directs the laser beam at various angles, allowing the scanner to gather data from multiple viewpoints [25,26]. The sensor within the scanner assesses the intensity of the laser beam as it reflects off the object, facilitating the creation of a point cloud that represents the object's surface [26]. One of the notable advantages of terrestrial LiDAR is its ability to capture highly precise and dense data points, enabling detailed representations of vegetation structure [26,27].

According to Niță [28], several of the Time-of-Flight Laser Scanning laser pulses generated by the LiDAR sensor facilitates the direct quantification of the spatial separation between the sensor and surrounding objects. However, most of these pulses yield singular return data. Most of the terrestrial perspective scanners are returned by the ground, and this can be utilized to derive high-resolution DEMs that capture the intricate topographic features of the Earth's surface [29,30]. By comparing the measurements obtained from LiDAR with satellite-derived products, scientists can identify inconsistencies, refine input data, and enhance the reliability of hydrological simulations [31–34].

While previous studies have documented the general accuracy of satellite DEMs, specific challenges related to their precision across varied topographic features and en-

vironmental conditions remain unaddressed. Additionally, the sources of error and bias inherent to different satellite products have not been comprehensively analyzed. This study addresses these gaps by focusing on precision discrepancies across topographical features and evaluating sources of error using terrestrial LiDAR data as a ground truth reference.

This research is dedicated to evaluating the precision of satellite DEM products through a comparative analysis with terrestrial LiDAR measurements. This study pursues a dual objective: firstly, to assess the accuracy of satellite-derived products by examining their alignment with terrestrial LiDAR data and secondly, to identify potential sources of error or bias within satellite-derived datasets. Additionally, this study seeks to explore the variability in DEM accuracy across different topographical features.

The integration of ground truth measurements obtained through terrestrial LiDAR serves as a crucial reference point for the validation and calibration of satellite-derived DEM data. By systematically identifying and quantifying discrepancies between these datasets, this study enhances the precision of satellite-derived inputs essential for hydrological modeling. This refined approach not only improves landscape representation and model reliability but also supports more accurate predictions and decisions in critical applications such as water resource management, flood forecasting, and ecosystem analysis.

2. Materials and Methods

2.1. Study Area and Data Collection

This study was conducted within the Nanului watershed, located in the central part of Romania, near the city of Brașov (EPSG 3844) (Figure 1). This watershed encompasses a mountainous region characterized by dense forests, steep hills, and narrow valleys, making it an ideal location for terrain modeling and comparison.

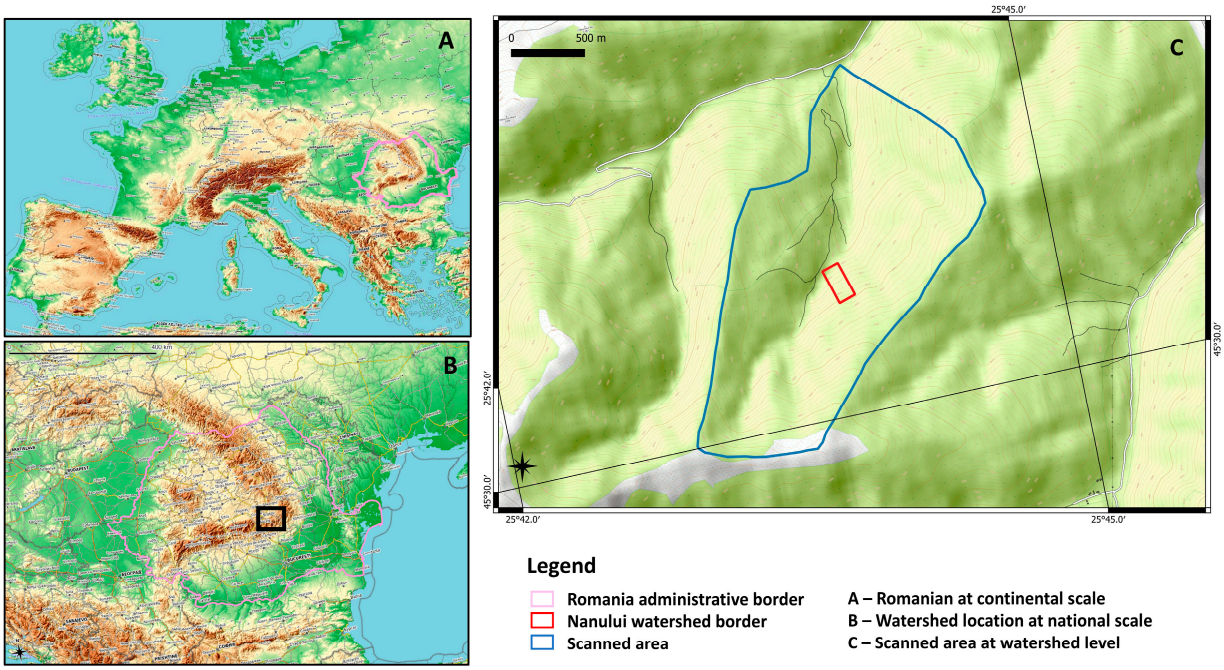

Figure 1. Geographical location of study area.

For this research, high-resolution terrestrial LiDAR data were collected systematically across the study area between July and October 2022 using a GeoSLAM Horizon scanner, developed and manufactured by GeoSLAM Ltd., headquartered in Nottingham, UK.

The GeoSLAM Horizon is a mobile terrestrial scanner (TLS) and operates based on the principle of emitting laser pulses and measuring the time it takes for the pulses to return after striking objects in the environment. The scanner's rotating mirror provides a 360-degree field of view, emitting laser pulses in all directions and capturing the reflected

signals with its sensors. As the scanner moves, it continuously collects data, generating a real-time 3D map using Simultaneous Localization and Mapping (SLAM) technology. A ZEB Horizon Scanner uses laser technology; weighing 1.3 kg, it is designed for outdoor applications that require scanning up to 100 m and at an accuracy of 1–3 cm. The resulting TLS dataset achieved a point density of approximately 1500 points per square meter, which was used to generate a high-resolution DEM with a spatial resolution of 0.2 m.

2.2. Satellite-Derived Products and Preprocessing

Alongside the TLS data, satellite-derived DEMs, specifically the ALOS World 3D (JAXA/ALOS/AW3D30_V1_1) and SRTM DEMs (USGS/SRTMGL1_003), were also used in this study for comparison. Both the ALOS and SRTM DEMs had an initial resolution of 30 m and were processed through Google Earth Engine (GEE). These satellite-derived DEMs were clipped to the study area to ensure they matched the spatial extent of the TLS data (Figure 2).

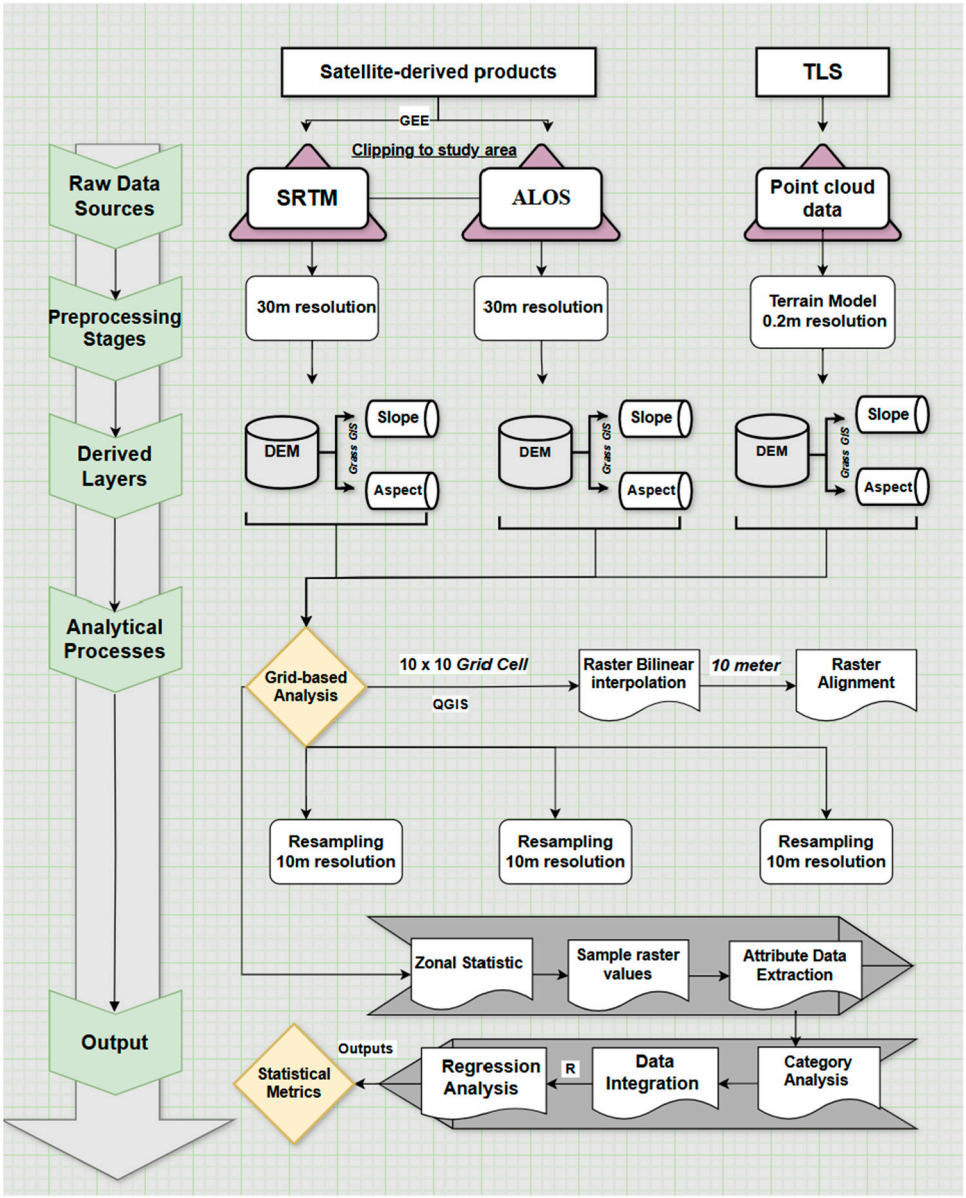

Figure 2. Summary of data processing and analysis workflow.

For each of the three datasets—TLS, ALOS, and SRTM—further terrain analyses were performed using GRASS GIS software (version 7.8.3). This included the calculation of slope and aspect values. Slope values were derived to assess the steepness of the terrain, while aspect values provided the compass direction of the slopes, which helped in understanding the exposure of the landforms to solar radiation and other environmental factors.

To enhance the visualization of the DEM, slope, and aspect layers, specific parameters were defined. For DEM visualization, the elevation range was set between 0 and 4000 m. For slope visualization, the values ranged from 0° to 90°, with a grayscale color palette transitioning from black (flat) to white (steep). Aspect visualization used a range of 0° to 360°, representing the full compass circle.

2.3. Grid-Based Analysis

A grid-based approach [35,36] was employed to facilitate systematic comparison across the datasets. Since the TLS dataset has a high resolution of 0.2 m and the satellite-derived DEMs (ALOS and SRTM) have a resolution of 30 m, it was essential to standardize the resolution across all datasets for accurate comparison. All three raster layers were resampled to a uniform resolution of 10 m, which was also the size of the grid cells used in the analysis. The TLS DEM was downsampled to 10 m using bilinear interpolation [35,37], while the ALOS and SRTM DEMs were upscaled to 10 m using the same interpolation method (Figure 2).

The study area was divided into 231 grid cells, each measuring 10 × 10 m, corresponding to the resolution of the resampled datasets. This grid structure allowed for direct comparisons of terrain metrics [38,39] between the TLS, ALOS, and SRTM DEMs. To maintain spatial alignment, all datasets were reprojected to a unified spatial reference system (EPSG: 3844) and aligned to a common grid structure. This alignment ensured that the pixels of each raster layer corresponded precisely to the 10 × 10 m grid cells, enabling reliable spatial correspondence during the analysis.

2.4. Statistical Analysis

To evaluate terrain characteristics within each grid cell, zonal statistics were computed using QGIS's "Zonal Statistics" tool. The mean, minimum, maximum, and standard deviation values were calculated for elevation (Table 1), aspect (Table 2), and Slope (Table 3) from the TLS, ALOS, and SRTM datasets. These metrics provided a statistical summary of terrain features within each grid cell, facilitating detailed comparisons across datasets. Raster values corresponding to the central points of each grid cell were extracted from the three datasets using the "Sample Raster Values" algorithm in QGIS. This process resulted in a vector dataset, where terrain metrics were stored as attributes for each grid cell, enabling precise and localized comparisons.

Table 1. Statistical summary of three models' elevation values.

Elevation	Min	Max	Range	Sum	Mean	SD	Sum of Squares
TLS	1096	1207	110	729,085,112	1150.862	27.573	481,671,195
SRTM	1110	1208	98	561,433	1155.211	27.844	376,035.17
ALOS	1115	1218	103	568,018	1168.761	30.516	451,668.31

Table 2. Statistical summary of three models' aspect values.

Aspect	Min	Max	Range	Sum	Mean	SD	Sum of Squares
TLS	0	359.99	359.99	11,010,470	175.02	144.8	1,320,651,49
SRTM	0	356.97	356.97	138,335	284.63	108.5	5,718,039.34
ALOS	0	354.18	354.18	29,536,672	247.19	131.6	2,021,837,73

Table 3. Statistical summary of three models' slope values.

Aspect	Min	Max	Range	Sum	Mean	SD	Sum of Squares
TLS	0.01	89.7	89.6	18,494,101	29.39	12.4	973,378
SRTM	3.69	30.1	26.4	9951.53	20.47	4.68	10,647
ALOS	0.49	45.2	44.7	10,923.47	22.47	6.57	20,955

Multiple linear regression models [40] were developed to examine how satellite-derived terrain parameters (slope, elevation, and aspect) correspond to their TLS-derived counterparts. These regression models allowed for the identification of significant relationships and potential discrepancies, providing insights into the accuracy of satellite DEMs.

For slope analysis, a multiple linear regression model was developed to quantify the influence of slopes derived from ALOS and the SRTM on TLS slopes. The model was structured as follows:

$$\text{TLS slope} = \beta_0 + \beta_1 \cdot \text{ALOS slope} + \beta_2 \cdot \text{SRTM slope} + \epsilon$$

where β_0 is the intercept term, representing the baseline value of the TLS slope when all independent variables are zero. β_1 and β_2 are the coefficients for the ALOS and SRTM slopes, respectively, capturing the magnitude and direction of their effects. ϵ represents the residual error, accounting for variance not explained by the model.

The regression coefficients were estimated using the least squares method, ensuring that the sum of squared differences between observed and predicted values was minimized. This model provided a basis for evaluating the relationships between satellite and TLS-derived slope metrics and identifying systematic differences.

To address the limitations and biases of individual datasets, a second analysis was conducted by integrating the SRTM and ALOS datasets. This integration aimed to enhance spatial coverage and improve elevation consistency prior to slope and aspect analyses. By combining the independent elevation sources, the merged DEM minimized gaps present in each dataset and accommodated variations in resolution and terrain coverage. The integration process was statistically validated using a one-way ANOVA test, which compared the elevation consistency of the merged dataset against individual datasets, ensuring the resulting DEM offered a more accurate terrain representation.

Model performance and statistical outcomes were evaluated using the root mean square error (RMSE) and adjusted R^2 The RMSE provided a measure of the average deviation between predicted and observed values, while the adjusted R^2 assessed the model's explanatory power, adjusting for the number of predictors.

3. Results

3.1. Regression Analysis of Elevation Datasets

A multiple linear regression analysis was performed to assess the relationship between TLS elevation and satellite-derived elevation datasets (SRTM and ALOS). The results demonstrated a highly significant association for both datasets with TLS elevation ($p < 2.2 \times 10^{-16}$). The model yielded an adjusted R-squared value of 0.955, indicating a strong correlation between TLS and the satellite-derived products. The residual standard error of 5.688 m provided a measure of the average deviation between predicted and observed TLS elevation values. These results confirm the robustness of the regression model and highlight the compatibility of satellite-derived elevation data with TLS measurements.

3.2. Individual Dataset Assessments

To evaluate the individual relationships between TLS elevation and each dataset, separate regression analyses were conducted (Table 4), in which the SRTM achieved an adjusted R-squared value of 0.955 and a root mean square error (RMSE) of 5.6520 m, reflecting its high precision and reliability in modeling TLS elevation. Meanwhile, ALOS exhibited a lower adjusted R-squared value of 0.8471 and an RMSE of 10.4346 m, indicating

reduced accuracy compared to the SRTM. The comparative analysis highlights the superior performance of the SRTM in accurately representing TLS elevation data, particularly in minimizing prediction errors (Table 1).

Table 4. Comparison of elevation models: TLS vs. SRTM and ALOS.

Model	R (Multiple R-Squared)	*p*-Value	RMSE
TLS elevation~ALOS elevation	0.8478	$<2.2 \times 10^{-16}$ (*** indicates highly significant)	10.48
TLS elevation~SRTM elevation	0.955	$<2.2 \times 10^{-16}$ (*** indicates highly significant)	5.688
TLS slope~ALOS slope	0.001771	0.5245 (not significant)	7.991
TLS slope~SRTM slope	0.1576	3.823×10^{-10} (*** indicates highly significant)	7.341
TLS aspect~ALOS aspect	0.2806	$<2.2 \times 10^{-16}$ (*** indicates highly significant)	65.54
TLS aspect~SRTM aspect	0.1369	6.586×10^{-9} (*** indicates highly significant)	71.79

Note: *** indicates highly significant ($p < 0.001$).

3.3. Comparing Elevation Datasets

A comparative analysis was performed between TLS, SRTM, and ALOS elevation data. (Figure 3). The results revealed significant differences among the three datasets based on a one-way ANOVA test (F = 30.95, $p = 1.35 \times 10^{-13}$). These differences emphasized notable variations in elevation values across datasets. To address the limitations of individual datasets, SRTM and ALOS data were merged. The merged DEM demonstrated a statistically significant improvement in terrain representation, validated by a one-way ANOVA test (F = 22.34, $p = 2.76 \times 10^{-6}$). This integration resulted in a more detailed and accurate elevation model, well suited for slope and aspect analyses.

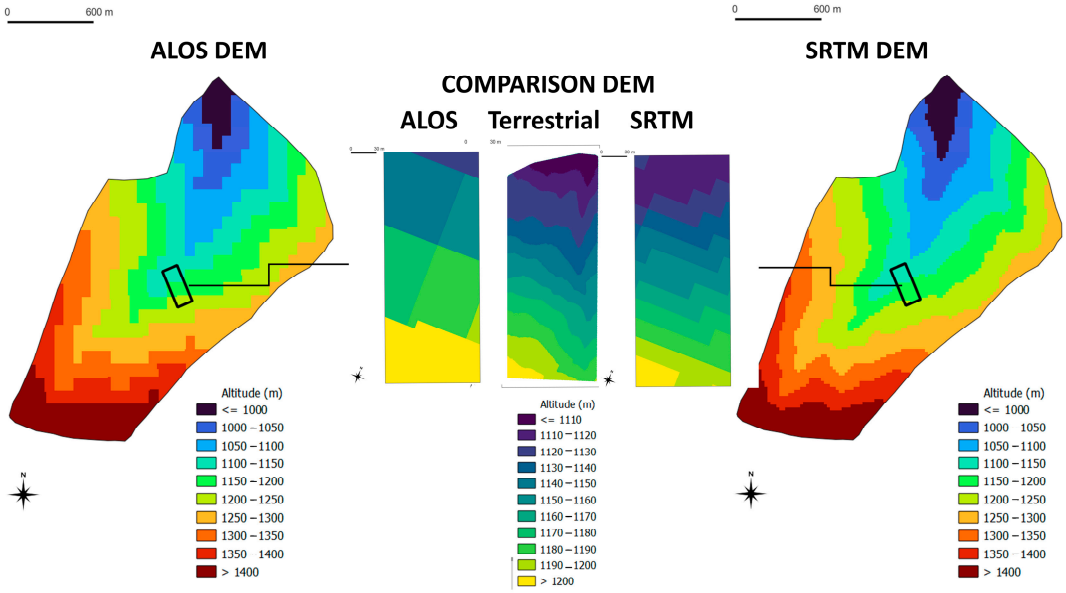

Figure 3. Analyzing the datasets using a grid-cell-based approach.

3.4. Statistical Analysis of Slope and Aspect Datasets

The relationship between TLS slope and each satellite-derived slope was assessed through linear regression. The model equation was developed as follows:

$$\text{TLS slope} = 45.27900 + 0.07717 \times \text{ALOS slope} - 0.89719 \times \text{SRTM slope}$$

The results indicated that the SRTM slope showed a significant negative effect on the TLS slope ($t = -6.52$, $p = 4.47 \times 10^{-10}$), while the ALOS slope did not demonstrate a statistically significant relationship with the TLS slope ($t = 0.52$, $p = 0.603$). The intercept term was highly significant ($p < 2 \times 10^{-16}$), with an estimated value of 45.27900. The

adjusted R-squared value for the model was 0.1513, indicating that approximately 15.13% of the variation in the TLS slope could be explained by independent variables. The F-statistics (21.5, $p = 2.803 \times 10^{-9}$) confirmed the overall significance of the model. (Figures 4 and 5).

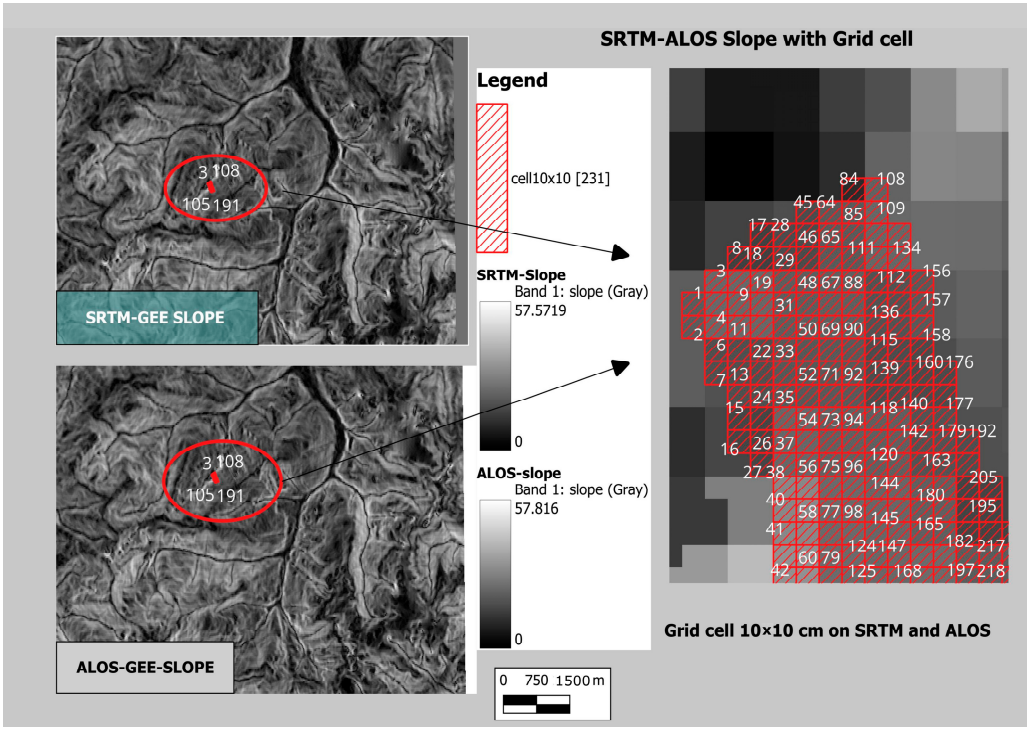

Figure 4. Slope analysis of satellite-derived products (ALOS and SRTM) using grid cell analysis.

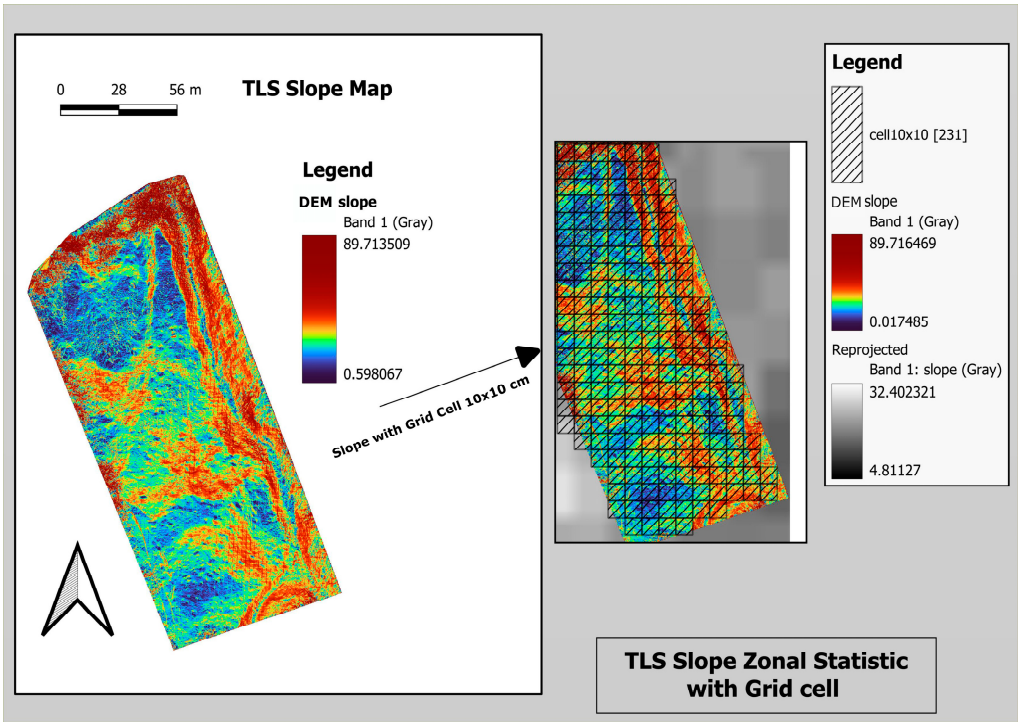

Figure 5. Analyzing the TLS slope using a grid-cell-based approach.

In terms of aspect, the coefficient for ALOS aspect (0.24047) was statistically significant (t = 7.513, $p = 1.30 \times 10^{-12}$), indicating a strong positive relationship with TLS aspect. Similarly, the coefficient for SRTM aspect (0.13403) was also significant (t = 3.017, $p = 0.00285$), showing a positive relationship, though weaker than that of ALOS. The intercept term was highly significant (t = 6.422, $p = 7.72 \times 10^{-10}$). The adjusted R-squared value of 0.3021 suggested that the independent variables explained approximately 30.21% of the variation in the TLS aspect. The overall model fit was confirmed by an F-statistic of 50.79 and a p-value of less than 2.2×10^{-16}, highlighting the significance of the model (Figures 6 and 7).

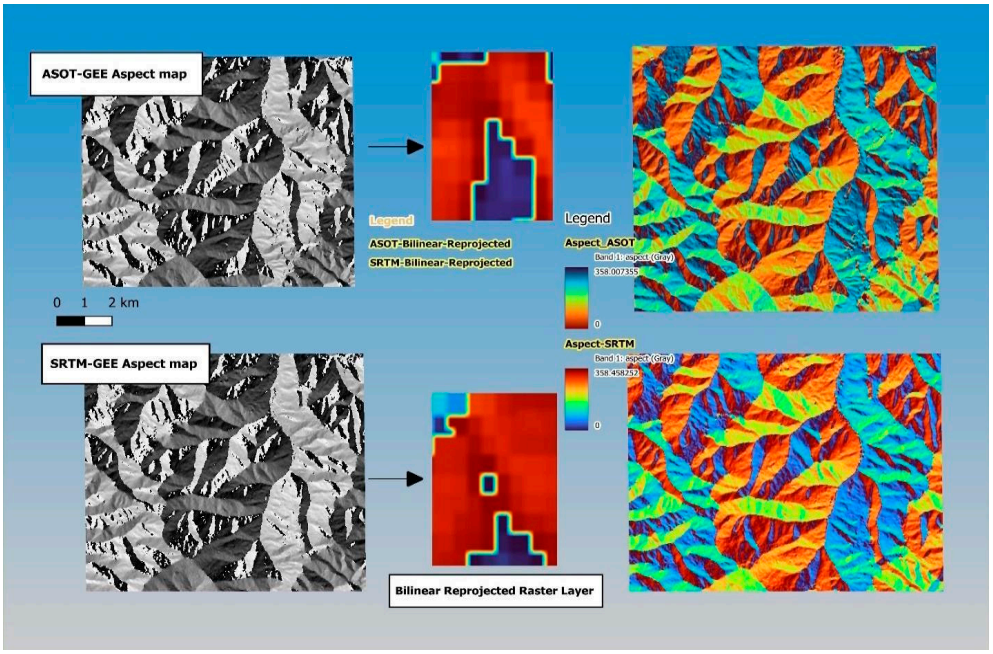

Figure 6. Aspect analysis of satellite-derived products (ALOS and SRTM).

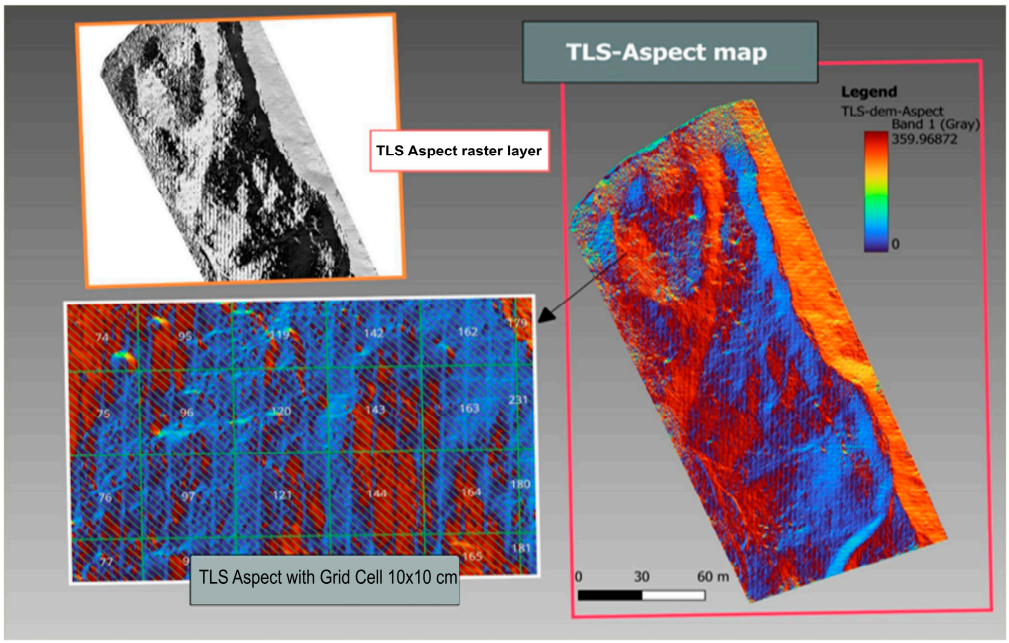

Figure 7. Analyzing the TLS aspect using a grid-cell-based approach.

4. Discussion

Our study aimed to assess accuracy in satellite DEMs by utilizing high-resolution Light Detection and Ranging data for terrain modeling. Our primary objective was to identify and evaluate discrepancies between satellite-derived elevation data and LiDAR measurements, providing valuable insights into the accuracy of elevation correlation. Through regression analysis, we observed a strong and statistically significant correlation between elevation values derived from the SRTM and ALOS datasets in comparison to TLS measurements. The obtained coefficients, featuring highly significant *p*-values, underscored the reliability of this correlation. In the upcoming sections, we will explore in more detail the accuracy of satellite-derived elevation models, clarifying the significance of the high adjusted R-squared value. Furthermore, we will examine individual relationships, offering comprehensive insights into the accuracy of each satellite-derived product. Our analysis of slope and aspect measurements beyond elevation revealed specific relationships with terrain characteristics. These results lay the groundwork for future research, suggesting paths for a more comprehensive terrain analysis that integrates diverse data sources and explores the potential of data fusion for applications in environmental monitoring and disaster management.

4.1. Elevation Correlation and Accuracy

The results of our regression analysis revealed a significant correlation between elevation values derived from both the SRTM and ALOS datasets and those obtained through TLS measurements. Notably, the estimated coefficients for the SRTM and ALOS were 1.012162 and -0.009826, respectively, with highly significant *p*-values. This empirical evidence underscores the strong relationship between satellite-derived datasets and TLS ground truth measurements. Furthermore, the elevated adjusted R-squared value of 0.955 emphasizes the strength of this correlation, verifying the ability of satellite-derived elevation models to accurately represent the elevation information elucidated by TLS measurements. The residual standard error, measured at 5.688, serves as an average indicator of the deviation between predicted and actual TLS-derived elevation values, offering insights into the accuracy inherent in satellite-derived elevation products.

Furthermore, separate linear regression analyses were conducted to assess the individual relationships between TLS elevation and each satellite-derived product. The regression analysis for ALOS elevation revealed a coefficient estimate of 0.86039, accompanied by a highly significant *p*-value. Similarly, the regression analysis for SRTM elevation produced a coefficient estimate of 1.00199, also with a highly significant *p*-value. Both regression models exhibited robust relationships between the satellite-derived elevations and TLS elevations, as exemplified by the substantial adjusted R-squared values (0.8478 for ALOS and 0.9551 for SRTM).

In-depth insights into the accuracy of these relationships were provided by the root mean square error (RMSE) values. For ALOS elevation, the RMSE value was calculated at 10.4346, quantifying the average discrepancy between the satellite-derived product and TLS measurements. A lower RMSE suggests a higher level of agreement between the datasets, affirming the degree of accuracy achieved. Conversely, for SRTM elevation, the RMSE value was notably lower at 5.6520, indicating a smaller average difference between the satellite-derived model and TLS data, further corroborating the high accuracy of the satellite-derived elevation products.

4.2. Comparison of Slope and Aspect Measurements

Expanding our analysis beyond elevation, we conducted a comparative examination of slope and aspect measurements. The findings uncovered specific relationships: the SRTM-derived slope exhibited a noteworthy negative impact on the TLS-derived slope, whereas the relationship between the ALOS-derived slope and TLS slope did not manifest as statistically significant. The absence of a significant association between the ALOS slope and the TLS slope can be attributed to several potential factors. Firstly, disparities in

measurement resolution are a plausible contributor. TLS offers high-resolution measurements that meticulously capture slope characteristics within a confined area surrounding the scanner. It leverages direct laser beam measurements, thus detecting fine-scale terrain intricacies. In contrast, ALOS slope data may originate from satellite imagery at a coarser resolution, potentially resulting in discrepancies between the measured values and contributing to the observed lack of statistical significance.

Moreover, the different sensing methods used for ALOS and TLS slope measurements may lead to variations in measurement accuracy. In our investigation, slope values were obtained through two processes: resampling and applying the slope equation using GISs. The observed variability in measurements can be linked to the inherent differences in these methods. This emphasizes the need to comprehend the intricacies of data acquisition techniques, as they can notably impact measurement accuracy. These distinct sensing approaches could also amplify the disparities in the observed associations. Another factor to consider is the inherent variability in terrain features. ALOS-derived slope data and TLS-derived slope data may encapsulate different aspects of terrain characteristics. TLS primarily focuses on capturing the slope of individual trees or localized terrain features, while ALOS slope data tend to represent larger-scale slope variations. This inherent distinction in scale and underlying terrain features may well account for the observed lack of a significant association between the two variables.

Additionally, unaccounted variables, such as vegetation cover, soil type, and land use, may have influenced the relationship between the ALOS slope and the TLS slope. It is plausible that these additional factors could have a more pronounced impact on TLS-derived slope measurements, thus contributing to the absence of a statistically significant association with ALOS-derived slope data.

The statistical summary of slope values (Table 3) highlights the variability across the datasets. TLS-derived slope values have a mean of 29.39° and a standard deviation of 12.4°, indicating a wide range of terrain steepness captured at high resolution. In contrast, ALOS and the SRTM demonstrate lower means of 22.47° and 20.47° with standard deviations of 6.57° and 4.68°, respectively, the distribution of slope values reflecting the limitations in capturing finer topographic details. The underestimation of steeper slopes by both satellite models, evident in Figure 8b, underscores the challenges posed by their coarser resolution.

For aspect, the comparison reveals distinct patterns. The TLS dataset, with a mean aspect of 175.02° and a standard deviation of 144.8°, encapsulates detailed directional variations. In contrast, ALOS and the SRTM show higher means of 247.19° and 284.63° and lower standard deviations of 131.6° and 108.5°, respectively (Table 2). These differences align with the inherent smoothing effect of satellite models, as observed in Figure 8c. While both satellite datasets align well with TLS in homogeneous terrains, their performance struggles in areas of complex topography. This suggests potential for refinement in processing algorithms to better capture localized directional variability.

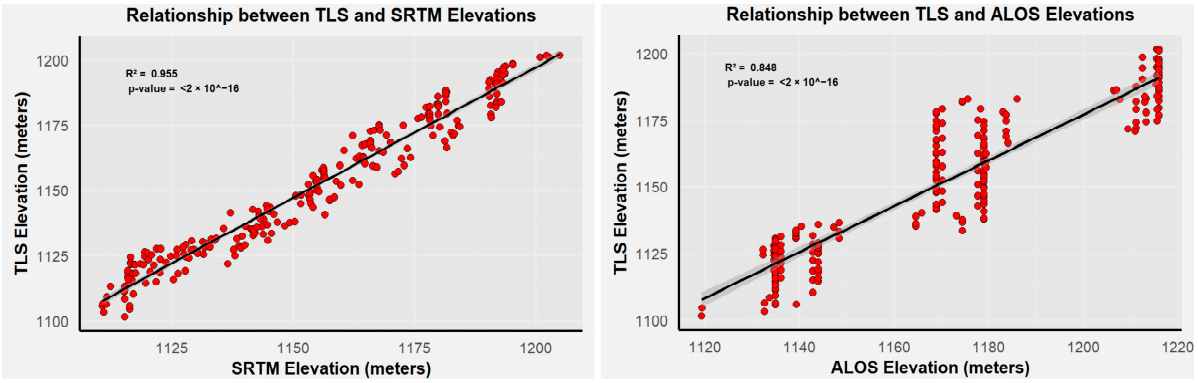

(**a**)

Figure 8. *Cont.*

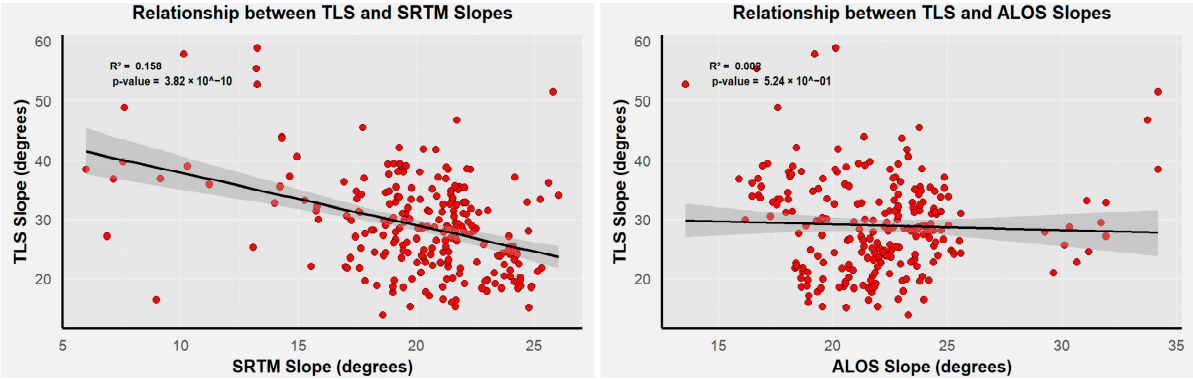

(**b**)

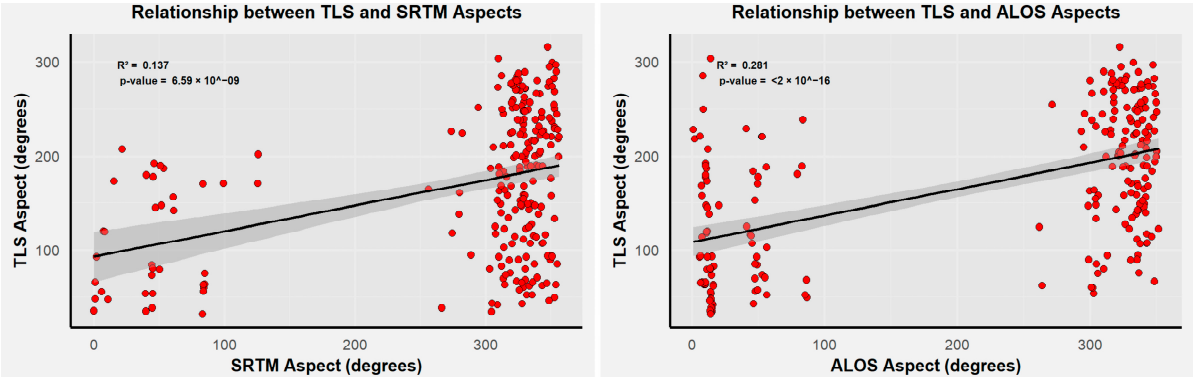

(**c**)

Figure 8. Comparison of satellites (SRTM and ALOS) with TLS measurements. (**a**) Elevation values, (**b**) slope values, and (**c**) aspect values for comparison of each model.

5. Conclusions

This study evaluated the accuracy of satellite-derived DEMs (SRTM and ALOS) in comparison to high-resolution terrestrial LIDAR (TLS) data. The results show that the SRTM DEM provides more accurate elevation data, with an adjusted R^2 of 0.955 and an RMSE of 5.65 m, compared to ALOS, which showed a lower adjusted R^2 of 0.847 and an RMSE of 10.43 m. While both satellite-derived DEMs showed a positive correlation with TLS aspect data, only the SRTM demonstrated a significant correlation with TLS slope data, highlighting its better performance in representing slope variations. These findings suggest that the SRTM DEM is a more reliable choice for applications requiring precise elevation and slope data, such as hydrological modeling and terrain analysis. The lower accuracy of ALOS in slope modeling suggests the need for further refinement, potentially through the integration of additional data sources or improved preprocessing techniques.

Moving forward, a key area for further investigation is the temporal analysis of terrain attributes using both satellite and terrestrial data. By examining changes in elevation, slope, and aspect over different time periods (e.g., seasons, years), future studies can uncover dynamic trends and fluctuations that are not captured in static datasets. Temporal analysis can shed light on seasonal variations driven by processes such as vegetation growth, snow accumulation, and erosion, as well as long-term trends related to land use changes or geological activity. This approach would add depth to our understanding of landscape evolution and improve the precision of terrain modeling.

Additionally, incorporating ancillary data sources, such as aerial imagery, hyperspectral data, and geophysical measurements, could further enhance the accuracy and applicability of DEMs. The integration of these diverse data types would allow for more robust cross-validation, offering a comprehensive view of terrain characteristics. Future studies can explore the potential of data fusion to improve the modeling of terrain features, such as elevation, slope, and aspect, across multiple data sources. This could lead to a more

detailed and accurate representation of the landscape, highlighting nuances that might be overlooked when relying on a single data source.

Author Contributions: Conceptualization, M.D.N. and A.H.M.; methodology, M.D.N.; software, M.I.K.; validation, M.D.N., A.H.M., and M.I.K.; formal analysis, A.H.M.; investigation, A.H.M.; resources, M.D.N.; data curation, M.I.K.; writing—original draft preparation, A.H.M.; writing—review and editing, M.D.N.; visualization, A.H.M. and M.I.K.; supervision, M.D.N.; project administration, M.D.N.; funding acquisition, M.D.N. All authors have read and agreed to the published version of the manuscript.

Funding: This research was funded by Transilvania University of Brasov PhD program.

Data Availability Statement: The original contributions presented in the study are included in the article, further inquiries can be directed to the corresponding authors.

Acknowledgments: We gratefully acknowledge the support of the anonymous reviewers who provided valuable comments that greatly improved this paper.

Conflicts of Interest: The authors declare no conflicts of interest.

References

1. Sharma, A.; Bagri, D.S. Comparison and Validation of Elevation Data at Selected Ground Control Points and Terrain Derivatives Derived from Different Digital Elevation Models. *Remote Sens. Earth Syst. Sci.* **2023**, *6*, 38–59. [CrossRef]
2. Kovanič, Ľ.; Blistan, P.; Urban, R.; Štroner, M.; Blišťanová, M.; Bartoš, K.; Pukanská, K. Analysis of the Suitability of High-Resolution DEM Obtained Using ALS and UAS (SfM) for the Identification of Changes and Monitoring the Development of Selected Geohazards in the Alpine Environment—A Case Study in High Tatras, Slovakia. *Remote Sens.* **2020**, *12*, 3901. [CrossRef]
3. Karlson, M.; Bastviken, D.; Reese, H. Error Characteristics of Pan-Arctic Digital Elevation Models and Elevation Derivatives in Northern Sweden. *Remote Sens.* **2021**, *13*, 4653. [CrossRef]
4. Guth, P.L.; Van Niekerk, A.; Grohmann, C.H.; Muller, J.-P.; Hawker, L.; Florinsky, I.V.; Gesch, D.; Reuter, H.I.; Herrera-Cruz, V.; Riazanoff, S.; et al. Digital Elevation Models: Terminology and Definitions. *Remote Sens.* **2021**, *13*, 3581. [CrossRef]
5. Tran, T.-N.-D.; Nguyen, B.Q.; Vo, N.D.; Le, M.D.; Nguyen, Q.B.; Lakshmi, V.; Bolten, J.D. Quantification of Global Digital Elevation Model (DEM)—A Case Study of the Newly Released NASADEM for a River Basin in Central Vietnam. *J. Hydrol. Reg. Stud.* **2023**, *45*, 101282. [CrossRef]
6. Bhardwaj, A.; Jain, K.; Chatterjee, R.S. Refining IKONOS DEM for Dehradun Region Using Photogrammetry Based DEM Editing Methods, Orthoimage Generation and Quality Assessment of Cartosat-1 DEM. *Environ. Sci. Proc.* **2020**, *5*, 3. [CrossRef]
7. Okolie, C.J.; Smit, J.L. A Systematic Review and Meta-Analysis of Digital Elevation Model (DEM) Fusion: Pre-Processing, Methods and Applications. *ISPRS J. Photogramm. Remote Sens.* **2022**, *188*, 1–29. [CrossRef]
8. Khanal, S.; KC, K.; Fulton, J.P.; Shearer, S.; Ozkan, E. Remote Sensing in Agriculture—Accomplishments, Limitations, and Opportunities. *Remote Sens.* **2020**, *12*, 3783. [CrossRef]
9. Moran, M.S.; Jackson, R.D. Assessing the Spatial Distribution of Evapotranspiration Using Remotely Sensed Inputs. *J. Environ. Qual.* **1991**, *20*, 725–737. [CrossRef]
10. Deijns, A.A.; Dewitte, O.; Thiery, W.; d'Oreye, N.; Malet, J.P.; Kervyn, F. Timing Landslide and Flash Flood Events from SAR Satellite: A Regionally Applicable Methodology Illustrated in African Cloud-Covered Tropical Environments. *Nat. Hazards Earth Syst. Sci.* **2022**, *22*, 3679–3700. [CrossRef]
11. Riquelme, A.; Ferrer, B.; Mas, D. Use of High-Quality and Common Commercial Mirrors for Scanning Close-Range Surfaces Using 3D Laser Scanners: A Laboratory Experiment. *Remote Sens.* **2017**, *9*, 1152. [CrossRef]
12. Jarihani, A.A.; Callow, J.N.; McVicar, T.R.; Van Niel, T.; Larsen, J. Satellite-Derived Digital Elevation Model (DEM) Selection, Preparation and Correction for Hydrodynamic Modelling in Large, Low-Gradient and Data-Sparse Catchments. *J. Hydrol.* **2015**, *524*, 489–506. [CrossRef]
13. Farr, T.G.; Rosen, P.A.; Caro, E.; Crippen, R.; Duren, R.; Hensley, S.; Kobrick, M.; Paller, M.; Rodriguez, E.; Roth, L.; et al. The Shuttle Radar Topography Mission. *Rev. Geophys.* **2007**, *45*, 1–33. [CrossRef]
14. Ivanova, Y.N.; Nafigin, I.O. Using the Landsat-8 Data Set and Shuttle Radar Topography Mission Digital Terrain Model for Gold–Polymetallic Mineralization Prediction on the Territory of the Central Part of the Malouralskaya Zone, the Polar Urals. *Izv. Atmos. Ocean. Phys.* **2023**, *59*, 1397–1408. [CrossRef]
15. Rabus, B.; Eineder, M.; Roth, A.; Bamler, R. The Shuttle Radar Topography Mission—A New Class of Digital Elevation Models Acquired by Spaceborne Radar. *ISPRS J. Photogramm. Remote Sens.* **2003**, *57*, 241–262. [CrossRef]
16. del Rosario González-Moradas, M.; Viveen, W.; Andrés Vidal-Villalobos, R.; Carlos Villegas-Lanza, J. A Performance Comparison of SRTM v. 3.0, AW3D30, ASTER GDEM3, Copernicus and TanDEM-X for Tectonogeomorphic Analysis in the South American Andes. *CATENA* **2023**, *228*, 107160. [CrossRef]

17. Wei, Y.; Gan, S.; Yuan, X.; Hu, L.; Gao, S. Analysis of Topographic Feature Parameters of Dinosaur Valley Ring Tectonic Geomorphology Based on the Advanced Land Observing Satellite Digital Elevation Model (ALOS DEM). *Appl. Sci.* **2023**, *13*, 13137. [CrossRef]
18. Khasanov, K.; Ahmedov, A. Comparison of Digital Elevation Models for the Designing Water Reservoirs: A Case Study Pskom Water Reservoir. *E3S Web Conf.* **2021**, *264*, 03058. [CrossRef]
19. Motohka, T.; Kankaku, Y.; Miura, S.; Suzuki, S. Overview of ALOS-2 and ALOS-4 L-Band SAR. In Proceedings of the 2022 IEEE Radar Conference (RadarConf22), Atlanta, GA, USA, 7–14 May 2021. [CrossRef]
20. Tabunshchik, V.; Gorbunov, R.; Gorbunova, T.; Pham, C.N.; Klyuchkina, A. Identification of River Basins within Northwestern Slope of Crimean Mountains Using Various Digital Elevation Models (ASTER GDEM, ALOS World 3D, Copernicus DEM, and SRTM DEM). *Front. Earth Sci.* **2023**, *11*, 1218823. [CrossRef]
21. Nikolakopoulos, K.G. Accuracy Assessment of ALOS AW3D30 DSM and Comparison to ALOS PRISM DSM Created with Classical Photogrammetric Techniques. *Eur. J. Remote Sens.* **2020**, *53*, 39–52. [CrossRef]
22. Short, N.; Brisco, B.; Couture, N.; Pollard, W.H.; Murnaghan, K.; Budkewitsch, P. A Comparison of TerraSAR-X, RADARSAT-2 and ALOS-PALSAR Interferometry for Monitoring Permafrost Environments, Case Study from Herschel Island, Canada. *Remote Sens. Environ.* **2011**, *115*, 3491–3506. [CrossRef]
23. Zou, L.; Wang, C.; Tang, Y.; Zhang, B.; Zhang, H.; Dong, L. Interferometric SAR Observation of Permafrost Status in the Northern Qinghai-Tibet Plateau by ALOS, ALOS-2 and Sentinel-1 between 2007 and 2021. *Remote Sens.* **2022**, *14*, 1870. [CrossRef]
24. Zhang, Y.; Hou, J.; Huang, C. Integration of Satellite-Derived and Ground-Based Soil Moisture Observations for a Precipitation Product over the Upper Heihe River Basin, China. *Remote Sens.* **2022**, *14*, 5355. [CrossRef]
25. Suchocki, C. Comparison of Time-of-Flight and Phase-Shift TLS Intensity Data for the Diagnostics Measurements of Buildings. *Materials* **2020**, *13*, 353. [CrossRef] [PubMed]
26. Wu, C.; Yuan, Y.; Tang, Y.; Tian, B. Application of Terrestrial Laser Scanning (TLS) in the Architecture, Engineering and Construction (AEC) Industry. *Sensors* **2021**, *22*, 265. [CrossRef]
27. Hancock, S.; McGrath, C.; Lowe, C.; Davenport, I.; Woodhouse, I. Requirements for a Global Lidar System: Spaceborne Lidar with Wall-To-Wall Coverage. *R. Soc. Open Sci.* **2021**, *8*, 211166. [CrossRef]
28. Niță, M.D. Testing Forestry Digital Twinning Workflow Based on Mobile LiDAR Scanner and AI Platform. *Forests* **2021**, *12*, 1576. [CrossRef]
29. Asner, G.P. Carnegie Airborne Observatory: In-Flight Fusion of Hyperspectral Imaging and Waveform Light Detection and Ranging for Three-Dimensional Studies of Ecosystems. *J. Appl. Remote Sens.* **2007**, *1*, 013536. [CrossRef]
30. Mazlan, S.M.; Jaafar, W.S.W.M.; Kamarulzaman, A.M.M.; Saad, S.N.M.; Ghazali, N.M.; Adrah, E.; Maulud, K.N.A.; Omar, H.; Teh, Y.A.; Dzulkifli, D. A Review on the Use of LiDAR Remote Sensing for Forest Landscape Restoration. *Remote Sens. Earth Syst. Sci.* **2022**, 49–74. [CrossRef]
31. Anand, V.; Oinam, B.; Parida, B.R. Uncertainty in Hydrological Analysis Using Multi-GCM Predictions and Multi-Parameters under RCP 2.6 and 8.5 Scenarios in Manipur River Basin, India. *J. Earth Syst. Sci.* **2020**, *129*, 223. [CrossRef]
32. Lin, S.; Jing, C.; Coles, N.A.; Chaplot, V.; Moore, N.J.; Wu, J. Evaluating DEM Source and Resolution Uncertainties in the Soil and Water Assessment Tool. *Stoch. Environ. Res. Risk Assess.* **2012**, *27*, 209–221. [CrossRef]
33. Moges, D.M.; Virro, H.; Kmoch, A.; Cibin, R.; Rohith, A.N.; Martínez-Salvador, A.; Conesa-García, C.; Uuemaa, E. How Does the Choice of DEMs Affect Catchment Hydrological Modeling? *Sci. Total Environ.* **2023**, *892*, 164627. [CrossRef] [PubMed]
34. Rocha, J.; Duarte, A.; Silva, M.; Fabres, S.; Vasques, J.; Revilla-Romero, B.; Quintela, A. The Importance of High-Resolution Digital Elevation Models for Improved Hydrological Simulations of a Mediterranean Forested Catchment. *Remote Sens.* **2020**, *12*, 3287. [CrossRef]
35. Habib, M. Evaluation of DEM Interpolation Techniques for Characterizing Terrain Roughness. *CATENA* **2021**, *198*, 105072. [CrossRef]
36. Maleika, W. The Influence of the Grid Resolution on the Accuracy of the Digital Terrain Model Used in Seabed Modeling. *Mar. Geophys. Res.* **2014**, *36*, 35–44. [CrossRef]
37. Xu, W.; Li, J.; Peng, D.; Yin, H.; Jiang, J.; Xia, H.; Wen, D. Vertical Accuracy Assessment and Improvement of Five High-Resolution Open-Source Digital Elevation Models Using ICESat-2 Data and Random Forest: Case Study on Chongqing, China. *Remote Sens.* **2024**, *16*, 1903. [CrossRef]
38. Kienzle, S. The Effect of DEM Raster Resolution on First Order, Second Order and Compound Terrain Derivatives. *Trans. GIS* **2003**, *8*, 83–111. [CrossRef]
39. Erskine, R.H.; Green, T.R.; Ramirez, J.A.; MacDonald, L.H. Digital Elevation Accuracy and Grid Cell Size: Effects on Estimated Terrain Attributes. *Soil Sci. Soc. Am. J.* **2007**, *71*, 1371–1380. [CrossRef]
40. Xu, W.; Li, J.; Peng, D.; Jiang, J.; Xia, H.; Wen, D. Comparison of Five Methods for Improving the Accuracy of SRTM3 DEM and TanDEM-X DEM in the Qinghai-Tibet Plateau Using ICESat-2 Data. *Int. J. Digit. Earth* **2024**, *17*, 2391036. [CrossRef]